Available online at www.sciencedirect.com
SCIENCE DIRECT®
International Journal of Heat and Mass Transfer 49 (2006) 3708–3716
International Journal of HEAT and MASS TRANSFER
www.elsevier.com/locate/ijhmt

The onset of longitudinal vortex rolls in the thermal entrance region of plane Poiseuille flow heated with a constant heat flux

Joung Hwan Park [a], Tae Joon Chung [a], Eun Suk Yun [a], Min Chan Kim [b], Chang Kyun Choi [a,*]

[a] School of Chemical and Biological Engineering, Seoul National University, Seoul 151-744, South Korea
[b] Department of Chemical Engineering, Cheju National University, Cheju 690-756, South Korea

Received 21 December 2004; received in revised form 10 January 2006
Available online 17 April 2006

Abstract

The onset of longitudinal vortex rolls in the thermal entrance region of plane Poiseuille flow heated from below with a constant heat flux is investigated theoretically. In the present study, the Boussinesq equations are solved numerically by using the finite volume method to analyze the onset of secondary flow. The local growth rates of the mean temperature and its fluctuations are examined, and the three characteristic distances, which are those to exhibit the onset of intrinsic instability, the detection of secondary flow, and the minimum Nusselt number under mixed convection, are suggested. They are discussed in comparison with available experimental data for water and air.

Keywords: Longitudinal vortex roll; Plane Poiseuille flow; Constant-flux heating; Local growth rate; Convective instability; Rayleigh number

1. Introduction

When a fluid layer between two horizontal plates is heated rapidly from below, natural convection sets in due to the buoyancy force. This buoyancy-driven convection can occur in a number of heat transfer systems where the primary flow of laminar forced convection exists, such as liquid film processes, flows in heat exchangers and chemical vapor deposition. Since most of these processes involve nonlinear developing temperature profiles, it is important to predict where secondary flow sets in.

For the linear temperature system of plane Poiseuille flow, Gage and Reid [1] showed that except very slow flow the stability criteria are the same as those of Rayleigh–Bénard convection. In the thermal entrance region of plane Poiseuille flow heated isothermally from below, Hwang and Cheng [2] first conducted stability analysis. Predictions of Lee and Hwang [3] and Kim et al. [4] agree well with the experimental results of Hwang and Liu [5], Kamotani and Ostrach [6] and Kamotani et al. [7]. But all the above models need a further justification.

For the specific case of the thermal entrance region of plane Poiseuille flow heated with a constant heat flux, Incropera and his colleagues [8–14] investigated the onset of secondary flow numerically and experimentally for water and air systems. They determined the related characteristic distances by flow visualization and heat transfer measurement. Ozsunar et al. [15,16] also conducted numerical and experimental analyses for the mixed convection in a horizontal and inclined channel. They measured only the heat transfer enhancement and investigated the effects of aspect ratio and channel inclination. As shown in the experiments of Maughan and Incropera [14] for air flow, there is a difference between the characteristic distances obtained by flow visualization and heat transfer measurement. The onset of instability would not be detected

* Corresponding author. Tel.: +82 2 880 7407; fax: +82 2 888 7295.
E-mail address: ckchoi@snu.ac.kr (C.K. Choi).

0017-9310/$ - see front matter © 2006 Elsevier Ltd. All rights reserved.
doi:10.1016/j.ijheatmasstransfer.2006.01.049

Nomenclature

a	dimensionless horizontal wavenumber
A, B	amplitudes of temperature and velocity fluctuations
E_1	energy functional of fluctuations
F_B	buoyancy force
g	gravitational acceleration constant [m s^{-2}]
H	thickness of the fluid layer [m]
k	thermal conductivity [W m^{-1} K^{-1}]
L	width of the cross-section [m]
Nu	Nusselt number, $q_w H/\{kT_w - T_i\}$
p	dimensionless pressure, $PH^2/(\rho_i \alpha^2)$
P	dynamic pressure [N m^{-2}]
Pe	Péclet number, $U_{av}H/\alpha$
Pr	Prandtl number, ν/α
q_w	heat flux at the bottom wall [W m^{-2}]
Ra_q	Rayleigh number based on the heat flux, $g\beta q_w H^4/(k\alpha\nu)$
r_0	local growth rate of mean quantities
r_1	local growth rate of fluctuations
Re	Reynolds number, $U_{av}H/\nu$
S	vertical area at each x [m^2]
T	temperature [K]
u_0	dimensionless basic velocity
$\mathbf{U}$	velocity vector, $\hat{\mathbf{i}}U + \hat{\mathbf{j}}V + \hat{\mathbf{k}}W$
U_{av}	average velocity [m s^{-1}]
$\mathbf{v}$	dimensionless velocity vector, $\hat{\mathbf{j}}v + \hat{\mathbf{k}}w$
v, w	dimensionless spanwise and vertical velocities, $(V, W)H/\alpha$
V, W	spanwise and vertical velocities [m s^{-1}]
x	dimensionless axial distance, $X/(PeH)$
X	streamwise distance [m]
y, z	dimensionless coordinates, $(Y, Z)/H$
Y, Z	spanwise and vertical distances [m]

Greek symbols

α	thermal diffusivity [m^2 s^{-1}]
β	volumetric thermal expansion coefficient [K^{-1}]
Δ_T	thermal penetration depth [m]
μ	viscosity [kg m^{-1} s^{-1}]
ν	kinematic viscosity [m^2 s^{-1}]
θ	dimensionless temperature, $k(T - T_i)/(q_w H)$
ρ	fluid density [kg m^{-3}]

Subscripts

*	normalized quantity
c	critical state
D	detection
i	inlet or initial state
m	maximum
rms	root-mean-square quantity
T	temperature
u	undershoot
V	velocity
w	bottom wall

Superscript

$'$	fluctuation

experimentally. Recently Kim et al. [17] employed the propagation theory and analyzed the convective instability problem for the present system. Their resulting critical distances constitute low bounds of scattered experimental data. This intimates that the growth of instability is needed for the manifestation of thermal convection.

In the present study, to examine the local behavior of convective instability, the three characteristic distances are suggested. They are the onset distance of convective instability, i.e., intrinsic instability, X_c, the detection distance of secondary flow, X_D, and the undershoot distance in the plot of Nusselt number vs. distance, X_u, where the minimum Nusselt number is exhibited. The critical distances illustrated by Kim et al. [17] describe the onset of convective instability to a certain degree. But their analyses based on the local stability analysis and propagation theory require a further justification. In addition, they did not show the local behaviors of thermal instabilities and the manifestation of mixed convection. Accordingly, in the present study, we will employ the finite volume method (FVM) and identify the above characteristic distances in comparison with the available experimental data of water and air.

2. Onset of vortex instabilities

2.1. Governing equations

The system considered here is the plane Poiseuille flow of a Newtonian fluid as shown in Fig. 1. The bottom plate is heated with a constant heat flux q_w, and the top plate is kept at a constant inlet temperature T_i. Here, the channel height is H, and the fluid flow has the fully-developed velocity profile. For a high q_w, in the thermal entrance region of laminar forced convection, the nonlinear developing temperature profiles are formed and the buoyancy-driven convection sets in at a certain distance in form of

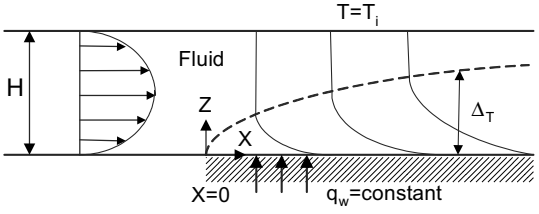

Fig. 1. Basic state of laminar forced convection.

regular longitudinal vortex rolls. The governing equations of the flow and temperature fields for the steady-state flow are expressed as follows:

$$\nabla \cdot \mathbf{U} = 0, \tag{1}$$

$$\rho_i \mathbf{U} \cdot \nabla \mathbf{U} = -\nabla P + \mu \nabla^2 \mathbf{U} + \rho g \hat{\mathbf{k}}, \tag{2}$$

$$\mathbf{U} \cdot \nabla T = \alpha \nabla^2 T, \tag{3}$$

where $\mathbf{U}$, P, T, ρ, μ, g and α denote, respectively, the velocity vector, the dynamic pressure, the temperature, the density, the viscosity, the gravitational acceleration constant, and the thermal diffusivity. Here, $\hat{\mathbf{k}}$ represents the vertical unit vector and ρ_i is the density at $T = T_i$.

For a large Péclet number $Pe(=U_{av}H/\alpha)$, the convective heat transfer dominates the conduction one in the streamwise direction. Here U_{av} is the average streamwise velocity and it is known that for large Pe longitudinal vortex rolls are observed experimentally [18,19]. When regular vortex rolls set in, the above three-dimensional (3D) governing equations are changed to the two-dimensional (2D) ones [17]. The latter ones are usually assumed near the onset of mixed convection for $Pe > 100$. The resulting dimensionless 2D governing equations are obtained with the Boussinesq approximation under the no-slip boundary conditions and the isothermal upper boundary:

$$\overline{\nabla} \cdot \mathbf{v} = 0, \tag{4}$$

$$u_0 \frac{\partial \mathbf{v}}{\partial x} + \mathbf{v} \cdot \overline{\nabla} \mathbf{v} = -\overline{\nabla} p + Pr \overline{\nabla}^2 \mathbf{v} + Pr Ra_q \theta \hat{\mathbf{k}}, \tag{5}$$

$$u_0 \frac{\partial \theta}{\partial x} + \mathbf{v} \cdot \overline{\nabla} \theta = \overline{\nabla}^2 \theta, \tag{6}$$

with the boundary conditions,

$$v = w = \frac{\mathrm{d}w}{\mathrm{d}z} = 0, \quad \frac{\partial \theta}{\partial z} = -1 \quad \text{at } z = 0, \tag{7a}$$

$$v = w = \frac{\partial w}{\partial z} = 0, \quad \theta = 0 \quad \text{at } z = 1, \tag{7b}$$

where $x = X/(PeH)$, $p = PH^2/(\rho_i \alpha^2)$, and $\theta = k(T - T_i)/(q_w H)$. Here $\mathbf{v}(= \hat{\mathbf{j}} v + \hat{\mathbf{k}} w)$ denotes the dimensionless velocity vector, where $\hat{\mathbf{j}}$ is the horizontal unit vector. The dimensionless axial velocity based on U_{av}, u_0, is expressed as the fully developed form of plane Poiseuille flow, i.e., $u_0 = 6(z - z^2)$, and the spanwise and vertical velocities, v and w, have the scale of α/H. The dimensionless Cartesian coordinates (y, z) have that of H, and the vector differential operator is denoted by $\overline{\nabla}(= \hat{\mathbf{j}}\partial/\partial y + \hat{\mathbf{k}}\partial/\partial z)$. The important parameters describing the present system, the Prandtl number Pr and the Rayleigh number Ra_q, are defined as

$$Pr = \frac{\nu}{\alpha}, \quad Ra_q = \frac{g\beta q_w H^4}{k\alpha\nu}, \tag{8}$$

where ν, β and k represent the kinematic viscosity, the thermal expansion coefficient, and the thermal conductivity, respectively.

In the present system, at the fully developed state, mixed convection exists for $Ra_q \geqslant 1296$. But in the thermal entrance region with $Ra_q \gg 1296$, the stability problem is complicated. The critical conditions of the incipient thermal instability in form of regular longitudinal vortex rolls were analyzed by the propagation theory [17], which is based on the assumption that incipient temperature disturbances are propagated mainly within the thermal boundary-layer thickness Δ_T at the onset distance of rolls. Therefore, all the variables and parameters having length scale are rescaled with Δ_T. The self-similar transformation is forced and the stability criteria are obtained easily. But the results obtained by this theory are approximate ones and they do not provide the detection distance of rolls. Accordingly, we will employ the numerical method.

2.2. Mean fields and fluctuations

The velocity and temperature fields are divided into the mean quantities and their fluctuations as follows:

$$\mathbf{v} = \langle \mathbf{v} \rangle + \mathbf{v}', \tag{9}$$

$$\theta = \langle \theta \rangle + \theta', \tag{10}$$

where $\langle \cdot \rangle$ and $'$ represent the mean quantities in the y-direction and their fluctuations, respectively. The mean quantity is a function of x and z, and it is known that $\langle \mathbf{v} \rangle = 0$ for regular even rolls.

In the present study the Nusselt number is defined as follows:

$$Nu = \frac{1}{L} \int_L \left(\frac{q_w H}{k(T_w - T_i)} \right)_{Z=0} \mathrm{d}Y, \tag{11}$$

where Y is the spanwise distance of the channel and L is the width of the cross-section. With secondary flow, Nu deviates from that of laminar forced convection and shows the minimum at $x = x_u$. The undershoot distance x_u is frequently used as the characteristic distance to identify the manifestation of secondary flow.

2.3. Local behavior of convective instability

In the present system secondary flow sets in due to the buoyancy force and its magnitude F_B is represented by

$$F_B = \rho_i g \beta |T - T_i|, \quad F_B = F_{B,0} + F_{B,1}, \tag{12a, b}$$

which are produced by temperature variations. Based on the dimensionless mean temperature and its fluctuations, the above buoyancy forces are written as

$$(F_{B,0}, F_{B,1}) = (\langle \theta \rangle, \theta') \rho_i g \beta q_w H/k. \tag{13}$$

In order to examine the local behavior of mixed convection along the streamwise distance x, the following local growth rates are defined:

$$r_{0,T} = \frac{1}{\langle \theta \rangle_{rms}} \frac{\mathrm{d}\langle \theta \rangle_{rms}}{\mathrm{d}x}, \tag{14}$$

$$r_{1,T} = \frac{1}{\theta'_{\mathrm{rms}}} \frac{\mathrm{d}\theta'_{\mathrm{rms}}}{\mathrm{d}x}, \tag{15}$$

where $r_{0,T}$ and $r_{1,T}$ are the local growth rates of the mean temperature and the temperature fluctuations, respectively. Here the subscript rms refers to the root-mean-square quantity, i.e., $(\cdot)_{\mathrm{rms}} = \sqrt{(\int_S (\cdot)^2 \mathrm{d}S)/S}$ with $\mathrm{d}S = \mathrm{d}y\,\mathrm{d}z$, where S represents the vertical area at each x. Similarly, we define the local growth rate of velocity fluctuations as follows:

$$r_{1,V} = \frac{1}{\mathbf{v}'_{\mathrm{rms}}} \frac{\mathrm{d}\mathbf{v}'_{\mathrm{rms}}}{\mathrm{d}x}, \tag{16}$$

where $\mathbf{v}'_{\mathrm{rms}} = [\int_S (v'^2 + w'^2)\mathrm{d}S/S]^{1/2}$. The spanwise and vertical velocities are generated by the work input of buoyancy forces.

2.4. Intrinsic instability

For the present distance-dependent problem the selection of the inlet conditions is very important. We do not know wherefrom disturbances exist and what kind of mode they would show, if any. According to experimental observations fluctuations are assumed to show periodic patterns as follows:

$$[\theta', \mathbf{v}'] \cong [A(x)\theta_*(z), B(x)\mathbf{v}_*(z)] \exp[\mathrm{i}(ay)] \quad \text{for } 0 \leqslant x \leqslant x_{\mathrm{c}}, \tag{17}$$

where $\mathrm{i} = \sqrt{-1}$. Here A and B are the amplitudes and x_{c} denotes the critical distance to mark the onset of instability. The functions θ_* and $\mathbf{v}_*$ represent the normalized temperature and velocity fluctuations, respectively. The inlet conditions at $x = 0$ are constructed as $\theta' = A(0)\theta_*(z)\cos(ay)$, $v' = -B(0)((\partial w_*(z)/\partial z)/a)\sin(ay)$ and $w' = B(0)w_*(z)\cos(ay)$, where $A(0)$ and $B(0)$ are the inlet amplitudes of fluctuations. Here it is assumed that for $0 \leqslant x \leqslant x_{\mathrm{c}}$, $\theta_*(z)$ and $w_*(z)$ would be formed somewhere by noises and the incipient patterns would not change. This means that the unique disturbance patterns are decided with the stability criteria.

The critical condition of the onset of intrinsic instability is suggested:

$$r_{1,T} = r_{0,T} \quad \text{with } r_{1,V} \geqslant 0 \quad \text{at } x = x_{\mathrm{c}}, \tag{18}$$

which means that the vortex instability of $a = a_{\mathrm{c}}$ that satisfies Eq. (17) sets in at the smallest distance x_{c}. It is stressed that the condition of $r_{1,V} \geqslant 0$ ensures the onset of instabilities. For $x < x_{\mathrm{c}}$, fluctuations are so small in comparison with the primary flow and they may be called noises. For $x > x_{\mathrm{c}}$, buoyancy-driven instabilities can grow and they are detected at some distance. Hereafter magnitude of fluctuations is comparable to that of the primary flow. Therefore, the system is assumed stable with $r_{1,T} < r_{0,T}$ but unstable with $r_{1,T} > r_{0,T}$. The above critical condition was first suggested by Choi et al. [20] in the time-dependent problem to analyze the onset of convective instabilty for the Rayleigh–Bénard convection.

3. Numerical simulation

We solved the governing equations and the boundary conditions (4)–(7) numerically using the FVM introduced by Patankar [21]. In the present study, only a regular longitudinal vortex roll with horizontal periodicity was considered. Accordingly, one convection roll with the symmetric side-boundary conditions was used to describe the horizontal infinite layer. The SIMPLE algorithm was used to solve the pressure equation connected with the continuity equation, and the hybrid scheme was employed to formulate the convection–diffusion discretization equation. In order to solve the present x-dependent problem, the implicit method was adopted and the first order x-increment was used. Also, to ensure the numerical stability, the distance step of $\Delta x = 10^{-7}$ was used. In the present x-dependent problem, the convergence was assumed when the changes of the velocities and temperature were smaller than 10^{-6} at each x-step.

For one vortex roll of $Ra_q = 10^7$ and $Pr \to \infty$, the number of meshes in the z-direction was examined to ensure numerical convergence: 20, 30, 40, 60 and 80. That in the y-direction was fixed at 42. At this condition the thermal boundary-layer thickness is very thin near $x = x_{\mathrm{c}}$. Therefore, finer meshes were used near the top and bottom boundaries to guarantee the physical validity. As shown in Fig. 2, the simulated temperature growth rate converged with the 60 z-meshes. Since the velocity one showed the same trend, the number of the vertical meshes on the plane was chosen as 42×60 in the present simulation. The above mesh numbers and the Δx size yielded almost the same temperature growth rate of the basic state, i.e., $r_{0,T}$ in laminar forced convection for $x \leqslant x_{\mathrm{c}}$ as the analytical one.

With the proper magnitude of the inlet temperature and velocity amplitudes $A(0)$ and $B(0)$, the present system was simulated numerically for a given Ra_q and Pr. The choice of the proper $A(0)$-value will be discussed in comparison

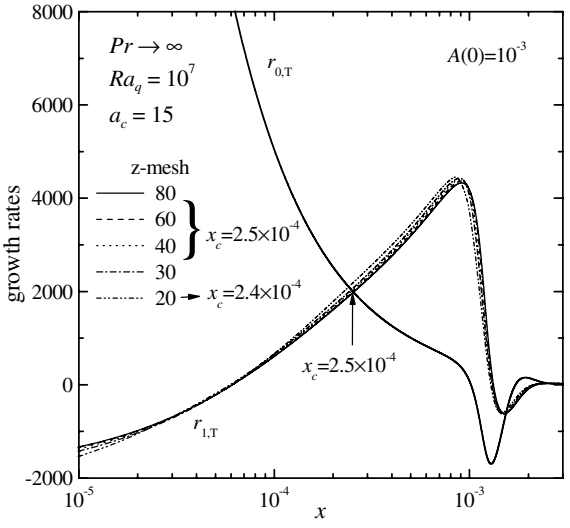

Fig. 2. Convergence test of temperature growth rates.

with the available experimental data. In the present study of plane Poiseuille flow, the numerical simulations were conducted for $Pr = 0.7$, 7 and $Pr \to \infty$. As a result, the x_c- and x_u-values for each case were obtained numerically.

In the present study, for the specific case of $Pr = 7$ and $Ra_q = 2.2 \times 10^7$, the 3D calculation was conducted by the commercial numerical simulation package FLUENT, which is also based on the FVM. The dimensional Eqs. (1)–(3) were solved. As the inlet condition, the inlet profile of the above 2D case was used. The 3D result agreed well with the 2D one, Eqs. (4)–(6).

4. Results and discussion

The results of numerical simulation by the FVM are reported here. The experimental data of Incropera and his colleagues [10–14] for water and air are compared with the present results. In the present study, only the onset of the regular longitudinal vortex roll is considered. Compared with the experimental data, the proper $A(0)$-values are chosen with $0 < A(0) < 10^{-2}$ and, based on Eqs. (14) and (15), the stability criteria satisfying the condition (18) are assumed to represent the fastest growing regular vortex instability, i.e., intrinsic instability.

4.1. The case of linear temperature

For the case of linear base temperature, the growing behavior of fluctuations is illustrated in Fig. 3 with its well-known critical conditions: $Ra_q = 1296$, $a_c = 2.55$, and $r_{0,T} = r_{1,T} = r_{1,V} = 0$ as $x_c \to \infty$. These stability criteria are independent of Pr and with these the fully-developed fluctuation patterns are the same as those from the propagation theory or local stability analysis. For a given Pr they constitute the unique paths of $r_{1,T}$ and $r_{1,V}$, as shown in the figure. They represent the fastest growing mode of regular longitudinal vortex rolls. Other patterns converge to these unique paths when the conditions (17) and (18) are satisfied iterating the calculations with the newly obtained patterns at the fully developed state. The other a-values finally show the decay of fluctuations with the negative $r_{1,T}$- and $r_{1,V}$-values, which means that the corresponding system is stable.

With decreasing Pr the growth rates of fluctuations increase and approach zero downstream. For the case of $Pr = 0.01$, the peculiar behavior of $r_{1,T} > 0$ for $0.1 < x \leqslant 1$ is observed before $r_{0,T} \to 0$. In the local stability analysis, the condition of $r_{1,T} = 0$ is forced as the critical condition of thermal instability. According to this theory there exist the two x_c-values to satisfy the condition of $r_{1,T} = 0$ for $Pr = 0.01$: $x_c = 0.13$ and ∞. However, the former value is not the critical condition to mark incipient instability because $r_{1,T} < r_{0,T}$ and $r_{1,V} < 0$. This violates the criterion (18) and the corresponding system is stable.

4.2. The case of $Pr \to \infty$

With $Ra_q = 10^7$, $Pr \to \infty$ and $A(0) = 10^{-4}$ the behavior of fluctuations along the streamwise distance is illustrated in Fig. 4. For small x, both w'_{rms} and θ'_{rms} retain almost the same magnitudes as their inlet ones but for $3 \times 10^{-4} < x < 10^{-3}$ they experience a sudden increase. The local growth rates given by Eqs. (14)–(16) are illustrated in Fig. 5. The instability criterion (18) yields $x_c = 2.5 \times 10^{-4}$ and $a_c = 15$ for $Ra_q = 10^7$, as shown in this figure. Here the $r_{1,T}$- and $r_{1,V}$-paths are the unique ones, which satisfy Eq. (17). The $r_{1,T}$-path is almost independent of the inlet velocity condition for $Pr \to \infty$. The maximum values of $r_{1,T}$ and $r_{1,V}$ appear at $x = x_{m,T}$ and $x_{m,V}$, respectively and for $x > x_{m,T}$, $r_{0,T}$ deviates from that of laminar forced convection. If there is no secondary flow, the relation of $r_{0,T} \geqslant 0$ is kept. Since secondary flow occurs due to

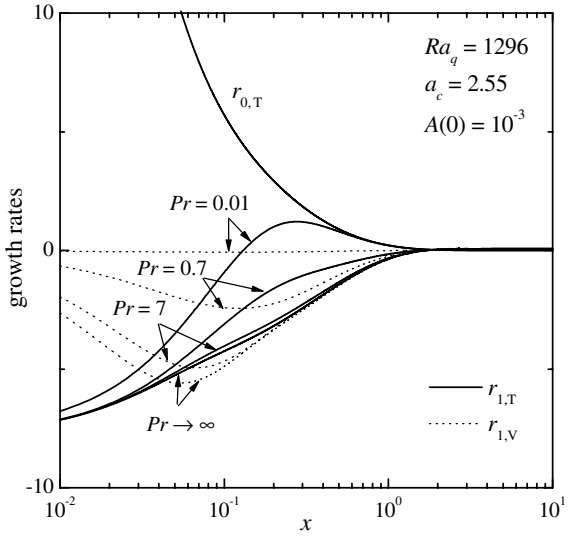

Fig. 3. Local growth rates for $Ra_q = 1296$.

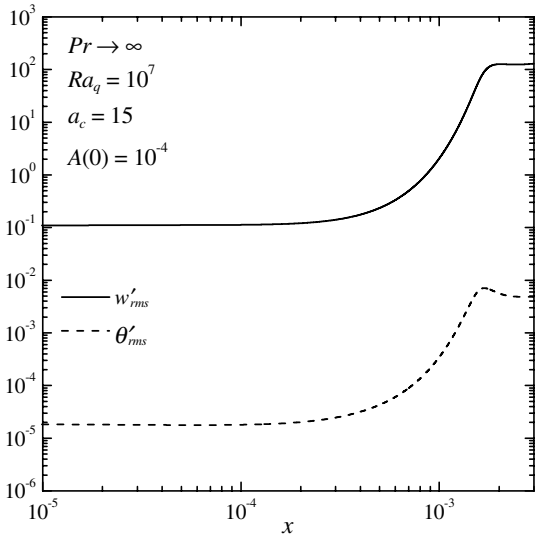

Fig. 4. Local behavior of fluctuations.

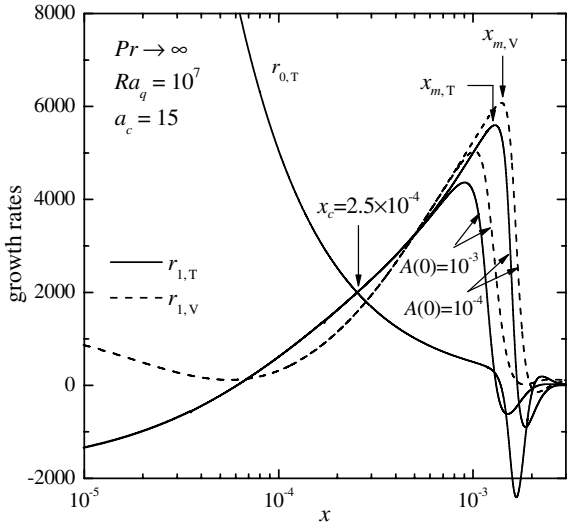

Fig. 5. Local growth rates for $Pr \to \infty$.

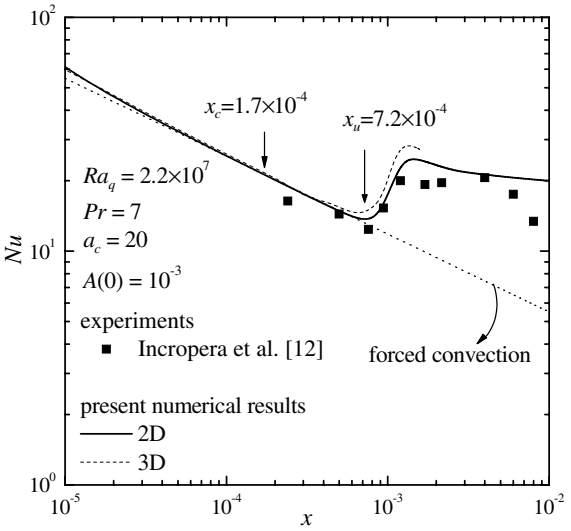

Fig. 6. Nusselt number vs. axial distance for $Pr = 7$.

temperature variations in the present buoyancy-driven convection, $r_{1,T}$ seems to play the critical role rather than $r_{1,V}$. In the amplification theory only the vertical velocity component of disturbances is examined. In the present model, the x_c-value is independent of the $A(0)$-value but $x_{m,T}$- and $x_{m,V}$-values are dependent upon its magnitude, as shown in Fig. 5. Therefore, it is stated that the present x_c-value is the invariant and therefore, it is here called the onset distance of intrinsic instability.

4.3. The case of Pr = 7

For water, the detection distance of mixed convection in the plane Poiseuille flow heated from below was investigated experimentally by Incropera and his colleagues [9–12]. The two characteristic distances were determined by both flow visualization and heat transfer measurement. The former distance indicates the position at which the dye injected ascends from the surface and the latter one does the position at which the Nusselt number deviates from that of laminar forced convection. The local behavior of the Nusselt number along the axial distance for $Ra_q = 2.2 \times 10^7$ and $Pr = 7$ is shown in Fig. 6. The present numerical simulation result with $A(0) = 10^{-3}$ is comparable with the experimental data. Also, the present 3D simulation is similar to the 2D one. For $Pr = 7$, the local growth rates of fluctuations ($r_{1,T}$ and $r_{1,V}$) are more distinguishable than those for $Pr \to \infty$, as shown in Fig. 7. The present results of $Pr = 7$ show that $x_u \cong x_{m,V}$. It is clear that manifest buoyancy-driven convection should exist at $x = x_u$.

For $Pr = 7$ the experimental data of Incropera and his colleagues [10–12] are summarized in Fig. 8. The experimental x_u-values are located between the numerical ones for $A(0) = 10^{-3}$ and 10^{-4}. With increasing Ra_q, the proper $A(0)$-value seems to decrease from 10^{-3} to 10^{-4}. The experimental x_D-values are located between x_c and x_u. Here it is evident that $x_c < x_D < x_u$ and the ratio of x_u to x_c is nearly

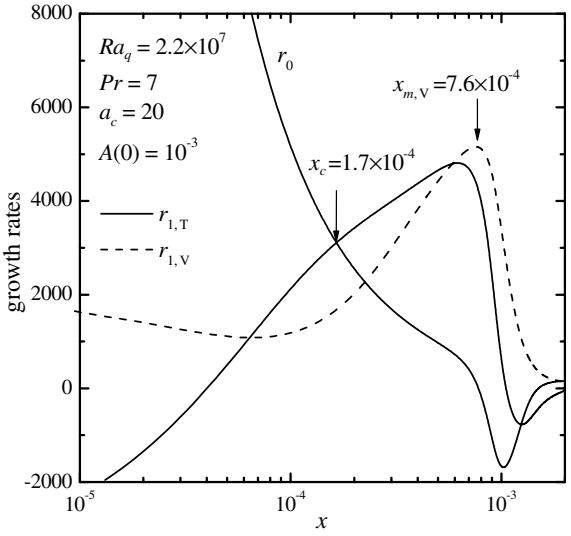

Fig. 7. Local growth rates for $Pr = 7$.

constant, which is dependent upon the $A(0)$-value. The Nusselt number starts to deviate from that of laminar forced convection at $x = x_D$, where secondary flow is also observed by flow visualization. But its definitive value is not clear. In the present numerical simulation for $Pr = 7$, the relations of $x_u \cong 4x_c$ and $x_u \cong 6x_c$, respectively, for $A(0) = 10^{-3}$ and 10^{-4} are shown. For $Ra_q < 3 \times 10^7$ the experimental x_u-value shows the relation of $x_u \cong 4x_c$ but that of $x_u \cong 6x_c$ is shown for $Ra_q > 10^8$. Therefore, it seems that the $A(0)$-value are dependent on the Rayleigh number.

4.4. The case of Pr = 0.7

In the present study, the numerical simulation was conducted for $Pr = 0.7$ and the results were compared with the experimental data of Maughan and Incropera [13,14] for airflow. They determined the detection distance of second-

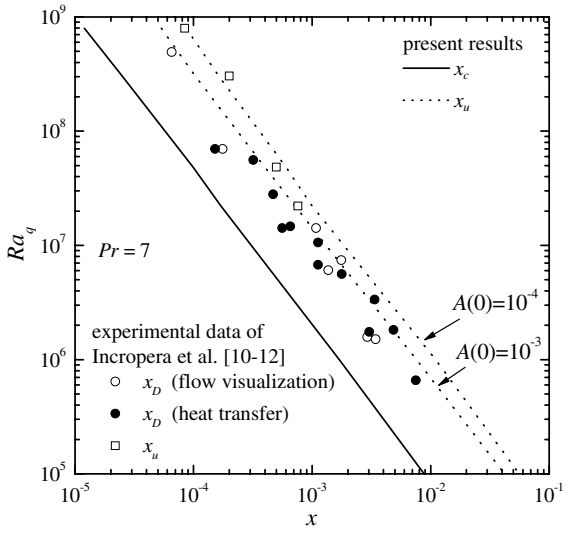

Fig. 8. Comparison of predictions with experiments for $Pr = 7$.

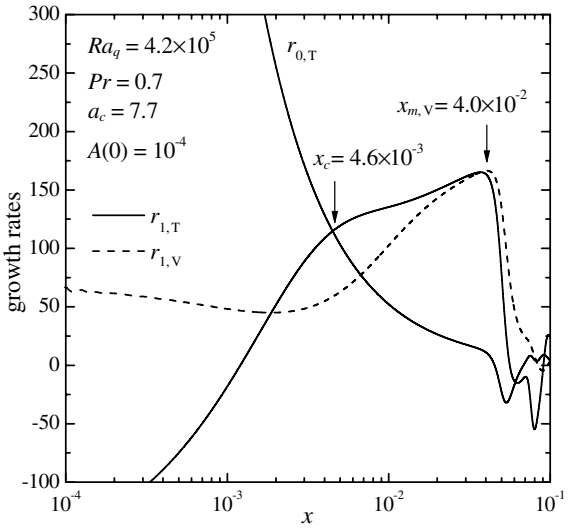

Fig. 10. Local growth rates for $Pr = 0.7$.

ary flow by flow visualization, observing the distance that the smoke injected begins to coalesce into several plumes on the bottom surface. For $Ra_q = 4.2\times10^5$ and $Pr = 0.7$ the numerical result of the Nusselt number with $A(0) = 10^{-4}$ is compared with the experimental data in Fig. 8. The predictions agree well with experimental results until they show an overshoot near $x = 7\times10^{-2}$. The local growth rates are illustrated in Fig. 10. Figs. 9 and 10 show that for $Pr = 0.7$, $x_{m,V} \cong x_u$ as well as the case of $Pr = 7$. The experimental data are compared with the present numerical results for $4\times10^4 < Ra_q < 10^7$ in Fig. 11, which shows that for airflow the detection distances by flow visualization are smaller than those by heat transfer measurement.

For $Pr = 0.7$, the proper $A(0)$-value seems to be 10^{-4} for the entire range of Ra_q measured, $4\times10^4 < Ra_q < 4\times10^5$. It is expected that the proper $A(0)$-value is also dependent

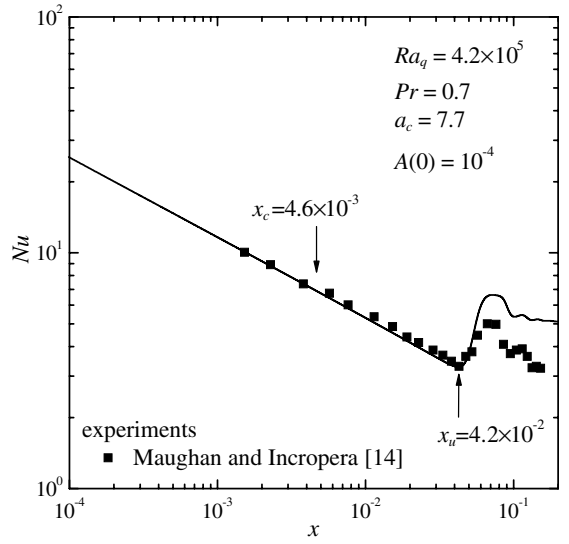

Fig. 9. Nusselt number vs. axial distance for $Pr = 0.7$.

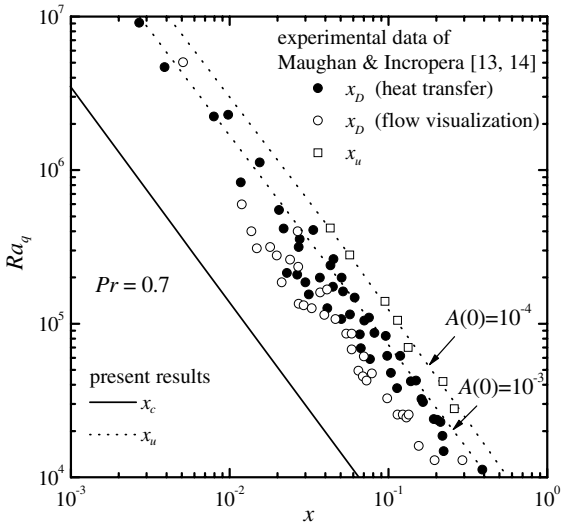

Fig. 11. Comparison of predictions with experiments for $Pr = 0.7$.

on Pr. The experimental x_D-values scatter more widely than those of $Pr = 7$ and it is shown that $x_c < x_D < x_u(\cong x_{m,V})$. Here the relation of $x_u \cong 9x_c$ is shown, which means that the growth of thermal instability is delayed for small Pr-value.

4.5. Discussion

The incipient instability may be very small and it will grow until secondary flow will be detected at $x = x_D$. In connection with the growth period to the manifestation of thermal convection in time-dependent Rayleigh–Bénard problems, Foster [22] suggested the amplification factor to exhibit manifest convection, which is the ratio of w'_{rms} to its initial value. But in the present system of $Pr \to \infty$, his amplification theory is invalid because the different inlet velocity condition yields the different amplification factor.

In the energy method which was introduced by Joseph [23], the measure to represent the convective instability is based on the energy functional of fluctuations, E_1:

$$E_1 = \frac{1}{2}\int_S \left(v'^2 + w'^2 + bPrRa_q\theta'^2\right)\mathrm{d}S, \tag{19}$$

which is composed of both the kinetic and the potential energy induced by buoyancy forces. In this method, the problem is that the definitive b-value is not known. The energy method usually yields a bound on the stability. It is known that Eqs. (15) and (16) are based on the individual energy quantities. It is noted that for $Pr \to \infty$ only the temperature term remains in Eq. (19).

The numerical simulation based on Eqs. (17) and (18) yields the onset distance of intrinsic instability. For $Ra_q > 10^4$, $Pe > 100$ and $20 < Re < 5000$, where $Re(=U_{av}H/\nu)$ is the Reynolds number, the critical conditions can be approximated by the following correlations:

$$x_c = 45Ra_q^{-3/4}, \quad a_c = 0.27Ra_q^{1/4} \quad \text{for } Pr \to \infty, \tag{20}$$

$$x_c = 56Ra_q^{-3/4}, \quad a_c = 0.29Ra_q^{1/4} \quad \text{for } Pr = 7, \tag{21}$$

$$x_c = 81Ra_q^{-3/4}, \quad a_c = 0.30Ra_q^{1/4} \quad \text{for } Pr = 0.7, \tag{22}$$

within the error bound of 10%. Here x_c is not sensitive on a near a_c and also on Pr for $Pr \geqslant 10$ [17]. For $Pr \geqslant 0.7$ the effect of Pr on a_c is not so large. The constants of above correlations are a little smaller than the results of Kim et al. [17], based on the propagation theory. It is mentioned that this theory yields a good approximation. For air experiments of $Re < 50$ transverse rolls can set in [24] and for small $Pe, \overline{\nabla}$ in Eqs. (4)–(6) should be replaced with the 3D operator. Therefore, the present simulation cannot be applied to the case of extremely small Pr and Re.

We do not know whether the inlet conditions exist or not. Thermal noises would set in somewhere downstream, among which the fastest growing mode of longitudinal vortex rolls will be formed following Eqs. (17) and (18). The above results show that the growth period is required until manifest mixed convection is detected. However, the experimental detection of secondary flow is not easy and it depends upon the respective experimental method to a certain degree. Therefore, the relation of $x_c < x_D < x_u \cong x_{m,V}$ is suggested here.

5. Conclusions

The critical distances to mark the onset of secondary flow in the thermal entrance region of plane Poiseuille flow have been investigated by using the FVM. For $Pr = 0.7$ and 7 the characteristic distances x_c, $x_{m,V}$ and x_u have been examined in comparison with available experimental data. In the present system, it is suggested that the fastest growing mode of regular vortex rolls sets in at $x = x_c$ with $r_{1,T} = r_{0,T}$. Here x_c is called the onset distance of intrinsic instability because it is the invariant. It is independent of $A(0)$-value. The manifestation of mixed convection is surely observed at the undershoot distance x_u, which is dependent upon the $A(0)$-value. When the available experimental data of $Pr = 7$ are examined, the proper $A(0)$-value moves from 10^{-3} to 10^{-4} with increasing Ra_q. For $Pr = 0.7$, the value of $A(0) = 10^{-4}$ looks proper. The choice of $A(0)$-value requires a further justification. The distance where secondary flow can be first detected, x_D, is located between x_c and x_u. Therefore, the relation of $x_c < x_D < x_u \cong x_{m,V}$ is suggested and linear theory is applied to $x < x_{m,V}$. The present numerical simulation follows actual phenomena reasonably well for $x_c \leqslant x < x_u$ and it also clarifies the characteristic distances x_c and x_u to a certain degree in connection with regular longitudinal vortex rolls.

Acknowledgement

This work was supported by LG Chemical Ltd., Seoul under the Brain Korea 21 Project of the Ministry of Education.

References

[1] K.S. Gage, W.H. Reid, The stability of thermally stratified plane Poiseuille flow, J. Fluid Mech. 33 (1968) 21–32.
[2] G.J. Hwang, K.C. Cheng, Convective instability in the thermal entrance region of a horizontal parallel-plate channel heated from below, J. Heat Transfer 95 (1973) 72–77.
[3] F.S. Lee, G.J. Hwang, Transient analysis on the onset of thermal instability in the thermal entrance region of horizontal parallel plate channel, J. Heat Transfer 113 (1991) 363–370.
[4] M.C. Kim, J.S. Baik, I.G. Hwang, D.-Y. Yoon, C.K. Choi, Buoyancy-driven convection in plane Poiseuille flow, Chem. Eng. Sci. 54 (1999) 619–632.
[5] G.J. Hwang, C.L. Liu, An experimental study of convective instability in the thermal entrance region of a horizontal parallel-plate channel heated from below, Can. J. Chem. Eng. 54 (1976) 521–525.
[6] Y. Kamotani, S. Ostrach, Effect of thermal instability on thermally developing laminar channel flow, J. Heat Transfer 98 (1976) 62–66.
[7] Y. Kamotani, S. Ostrach, H. Miao, Convective heat transfer augmentation in thermal entrance region by means of thermal instability, J. Heat Transfer 101 (1979) 222–226.
[8] F.P. Incropera, J.A. Schutt, Numerical simulation of laminar mixed convection in the entrance region of horizontal rectangular ducts, Numer. Heat Transfer 8 (1985) 707–729.
[9] D.G. Osborne, F.P. Incropera, Laminar mixed convection heat transfer for flow between horizontal parallel plates with asymmetric heating, Int. J. Heat Mass Transfer 28 (1985) 207–217.
[10] F.P. Incropera, A.L. Knox and J.A. Schutt, Onset of thermally driven secondary flow in horizontal rectangular duct, in: Proc. Eighth Int. Heat Transfer Conf., vol. 3, San Francisco, CA USA, 1986, pp. 1395–1400.
[11] J.R. Maughan, F.P. Incropera, Secondary flow in horizontal channels heated from below, Exp. Fluids 5 (1987) 334–343.
[12] F.P. Incropera, A.L. Knox, J.R. Maughan, Mixed-convection flow and heat transfer in the entry region of a horizontal rectangular duct, J. Heat Transfer 109 (1987) 434–439.
[13] J.R. Maughan, F.P. Incropera, Experiments on mixed convection heat transfer for airflow in a horizontal and inclined channel, Int. J. Heat Mass Transfer 30 (1987) 1307–1318.
[14] J.R. Maughan, F.P. Incropera, Regions of heat transfer enhancement for laminar mixed convection in a parallel plate channel, Int. J. Heat Mass Transfer 33 (1990) 555–570.
[15] A. Ozsunar, S. Baskaya, M. Sivrioglu, Numerical analysis of Grashof number, Reynolds number and inclination effects on mixed convec-

tion heat transfer in rectangular channels, Int. Commun. Heat Mass Transfer 28 (2001) 985–994.
[16] A. Ozsunar, S. Baskaya, M. Sivrioglu, Experimental investigation of mixed convection heat transfer in a horizontal and inclined rectangular channel, Heat Mass Transfer 38 (2002) 271–278.
[17] M.C. Kim, T.J. Chung, C.K. Choi, The onset of convective instability in the thermal entrance region of plane Poiseuille flow heated uniformly from below, Int. J. Heat Mass Transfer 46 (2003) 2629–2636.
[18] J.T. Lir, M.Y. Chang, T.-F. Lin, Vortex flow patterns near critical state for onset of convection in air flow through a bottom heated horizontal flat duct, Int. J. Heat Mass Transfer 44 (2001) 705–719.
[19] T.-F. Lin, Buoyancy driven vortex flow and thermal structures in a very low Reynolds number mixed convective gas flow through a horizontal channel, Int. J. Heat Fluid Flow 24 (2003) 299–309.
[20] C.K. Choi, J.H. Park, H.K. Park, H.J. Cho, T.J. Chung, M.C. Kim, Temporal evolution of thermal convection in an initially stably-stratified horizontal fluid layer, Int. J. Therm. Sci. 43 (2004) 817–823.
[21] S.V. Patankar, Numerical Heat Transfer and Fluid Flow, Taylor & Francis, New York, 1980.
[22] T.D. Foster, Onset of manifest convection in a layer of fluid with a time-dependent surface temperature, Phys. Fluids 12 (1969) 2482–2487.
[23] D.D. Joseph, Stability of Fluid Motions I and II, Springer-Verlag, New York, 1976.
[24] C.H. Yu, M.Y. Chang, T.F. Lin, Structure of moving transverse and mixed convection of air in a horizontal plane channel, Int. J. Heat Mass Transfer 40 (1997) 333–346.